Buoyancy Modes in a Low Entropy Bubble

F. R. Toffoletto[1], R. A. Wolf[1], and J. Derr[2]

[1]Physics and Astronomy Department, Rice University.

[2]Department of Physics and Nuclear Engineering, United States Military Academy.

Corresponding author: Frank Toffoletto (toffo@rice.edu)

Key Points:

- We investigate the properties of buoyancy modes in a low entropy bubble in the Earth's magnetosphere using a thin filament approach.
- We compare the frequencies and modes of these waves using: MHD ballooning theory, classic interchange theory, and an idealized formula.
- MHD ballooning theory finds 3 types of solutions in the bubble: interchange stable modes, unstable modes, and slow mode waves.

Abstract

In the nightside region of Earth's magnetosphere, buoyancy modes have been associated with low entropy bubbles. These bubbles form in the plasma sheet, particularly during substorm expansion, and move rapidly earthward and come to rest in the inner plasma sheet or inner magnetosphere. They often exhibit damped oscillations with periods of a few minutes and have been associated with Pi2 pulsations. In previous work, we used the thin filament approximation to compare the frequencies and modes of buoyancy waves using three approaches: magnetohydrodynamic (MHD) ballooning theory, classic interchange theory, and an idealized formula. Interchange oscillations differ from the more general MHD oscillations in that they assume a constant pressure on each magnetic field line. It was determined that the buoyancy and interchange modes are very similar for field lines that extend into the plasma sheet but differ for field lines that map to the inner magnetosphere. In this paper, we create a small region of entropy depletion in an otherwise stable entropy background profile of the magnetotail to represent the presence of a plasma bubble and determine the properties of the buoyancy modes using the same 3 approaches. In the bubble region, we find that in some regions the interchange and buoyancy modes overlap resulting in frequencies that are much lower than the background. In other regions within the bubble, we find interchange unstable modes while in other locations MHD normal mode predicts an MHD slow mode wave solution which is not found in the pure interchange solution.

Plain Language Summary

Low entropy plasma bubbles often form in the nightside region of the Earth's magnetosphere which move rapidly earthward and come to rest near the Earth. These bubbles often exhibit damped buoyancy oscillations with periods of a few minutes. Buoyancy waves are analogous to neutral-atmospheric gravity waves, in which the buoyant force is gravity rather than magnetic tension. This work seeks to better understand the properties of these oscillations. We use a thin filament approximation that assumes that magnetic field lines can be approximated by thin magnetic filaments that can slip through the background. We use three approaches: MHD ballooning theory, classic interchange theory, and an idealized plasma sheet formula to examine the properties of a small region of entropy depletion in the magnetotail to represent the presence of a plasma bubble. In the bubble region, we find that in some regions the interchange and buoyancy modes overlap, resulting in frequencies that are much lower than the background. On the Earthward edge of the bubble, we find regions of instability while on other locations within the bubbler that is furthest from the Earth the MHD normal mode predicts an MHD slow mode wave solution.

1 Introduction

In recent years there has been a change in our understanding of how plasma is transported from the plasma sheet to the inner magnetosphere. In the past, it was believed that steady earthward convection was the major transport mechanism. However, Erickson and Wolf (1980) pointed out that steady convection can lead to the 'pressure balance inconsistency' where empirical models of the magnetic field are not consistent with the assumption of entropy constancy in the plasma sheet seen in many early theoretical models. The theoretical assumption of entropy constancy was based on the bounce-averaged drift theory, where entropy is conserved along a drift path for an isotropic distribution function with isotropy sustained by strong, elastic pitch-angle scattering. Later it was recognized that

this inconsistency could be resolved with the presence of sporadic, bursty flows that are associated with low entropy bubbles (Pontius and Wolf, 1990; Yang et al., 2014). The existence of these bursty bulk flows has substantial observational support (e.g., Angelopoulos et al., 1992, 1994; Sergeev et al., 1996; Apatenkov et al., 2007). Using empirically based magnetic field and pressure models, the entropy $pV^{5/3}$, where p is the pressure and $V = \int ds/B$ is the flux tube volume, B is the magnitude of the magnetic field and s is the coordinate along the field line, it is often found to be a smooth background function of x_e, where x_e is the distance in the equatorial plane and increases sunward (i.e., $dpV^{5/3}/dx_e < 0$). In general, however, the magnetosphere probably has more structured entropy profiles as a function of position than such models show. While direct measurements of the entropy are not possible, it is possible to estimate the entropy using a technique developed by Wolf et al. (2006) which suggests that there is a lot of structure on the entropy in the tail. (e.g., Yang et al., 2010; Dubyagin et al., 2011; Sergeev et al., 2014). Some global MHD simulations also exhibit much structure in the entropy profile (e.g., Hu et al., 2011; Pembroke et al., 2012; Wiltberger et al., 2015; Cramer et al., 2017; Sorathia et al., 2021). The motivation of the work presented here is to examine the properties of MHD buoyancy waves when there is a localized reduction of the entropy.

The occurrence of plasma flows as they reach their equilibrium location has been associated with magnetohydrodynamic (MHD) buoyancy waves which are a fundamental wave mode of the magnetosphere. A bubble is an entropy-depleted plasma-sheet filament; i.e., it has reduced $pV^{5/3}$ relative to surroundings. The bubble moves Earthward toward its equilibrium position, where its entropy matches that of the local background environment (Birn et al., 2004; Xing and Wolf, 2007). The bubble often overshoots its equilibrium position and oscillates a few times (Chen and Wolf, 1999) as a buoyancy wave (Wolf et al., 2012; Toffoletto et al., 2020, 2022). Buoyancy waves are analogous to neutral-atmospheric gravity waves, in which the buoyant force is gravity rather than magnetic tension. Magnetospheric buoyancy waves are possibly related to Pi2 oscillations (Hsu and McPherron, 2007; Panov et al., 2010; Xing et al., 2015; Wang et al., 2020; Yadav et al. 2023).

To better understand the properties of low entropy bubbles, Chen and Wolf (1993, 1999) developed an MHD thin filament model to investigate their properties. The thin filament approach represents a highly idealized approximation to the motion of a field line in a plasma sheet background at equilibrium. This total filament pressure $p + B^2/2\mu_0$ balances the background. The thin filament approximation can be expressed as the solution of 1-D MHD equations that can be accurately solved with little dissipation (Chen and Wolf, 1999). In that work, it was found that a depleted filament overshoots its equilibrium point, where its entropy matches the background value, and undergoes damped oscillations about that location. In a follow-up study, Wolf et al. (2012) derived an approximate formula for the period of the fundamental oscillation frequency of a thin plasma sheet filament for a 2-D force-balanced tail model:

$$\omega^2 \approx (0.074\ s^{-2}) \left(\frac{\left(pV^{5/3}\right)'}{pV^{5/3}} \right)_e \frac{\left(T_{i,keV}\right)}{B_{z,e} V \left(1 + \frac{5}{6}\langle\beta\rangle\right)} \tag{1}$$

where $T_{i,keV}$ is the ion temperature in keV, $B_{z,e}$ is the strength of the z-component of the magnetic field, and $\langle\beta\rangle$ is the field line averaged plasma beta ($\beta \equiv 2\mu_0 p/B^2$). The prime

denotes a radial derivative. Henceforth, we will denote equation 1 as Wolf2012. The averaging is weighted by the flux tube volume, so that the field line average of a quantity A is:

$$\langle A \rangle \equiv \frac{\int A \frac{ds}{B}}{\int \frac{ds}{B}} . \quad (2)$$

Wolf2012, in agreement with much previous work on interchange stability (e.g, Bernstein et al., 1958), predicts that ω^2 is proportional to the entropy gradient and that the system is interchange unstable if the gradient is negative (i.e., $pV^{5/3}$ decreases away from the Earth). Panov et al. (2013) compared the results from the Wolf2012 equation with periods measured for 20 flow burst braking-oscillation events and found reasonably good agreement. This interchange oscillation formula, although derived for a very simple case, appears to be useful far beyond the constraints assumed in its derivation.

Toffoletto et al. (2020) used an MHD normal mode analysis to determine the buoyancy frequencies and eigenmodes of an oscillating thin filament. The approach was based on a linear approximation and assumed that the perturbations have time dependence of the form $e^{-i\omega t}$. Infinite conductance boundary conditions were assumed at the ionospheric footprints. The resulting two coupled equations of motion for the perpendicular and parallel displacements of mass points along the filament were solved as an eigenvalue problem to obtain the associated eigenfrequencies and eigenmodes. This approach differed from other approaches that looked at both poloidal and toroidal Alfvén and slow mode waves (e.g., Ohtani et al., 1989; Xia et al., 2017; Petrashchuk et al., 2022) that assumed low plasma beta configurations ($\beta < 1$) and a dipolar magnetosphere. Toffoletto et al. (2020) used the MHD normal analysis to determine the lowest frequency poloidal modes that were symmetric about the equatorial plane. They found that for field lines that map deep into the plasma sheet ($|x_e| > 15\ R_E$), these modes were buoyancy modes while field lines that mapped closer to the Earth (inside $|x_e| \sim 6\ R_E$) resembled slow mode waves. They also found that the predicted buoyancy frequencies were in surprisingly good agreement with the frequencies predicted by Wolf2012, even though this formula used a much less rigorous approach and was derived for the plasma sheet.

To better understand the relationship between MHD buoyancy modes and interchange, Toffoletto et al. (2022) looked at pure interchange modes and compared them to the less constrained MHD normal mode analysis. Using an energy approach like that of Bernstein et al. (1958), a buoyancy frequency for the interchange modes was derived by assuming that the oscillations are the result of the exchange of two adjacent field lines. The frequency for pure interchange oscillation was obtained as:

$$\omega_{PI}^2 = \frac{p}{\rho} \frac{\left(\frac{p_e'}{p} + \frac{5}{3}\frac{V_e'}{V}\right)\left(\frac{V_e'}{V} - \frac{\langle\beta\rangle}{2}\frac{p_e'}{p}\right)}{\left(1 + \frac{5}{6}\langle\beta\rangle\right)\langle\frac{\xi_\perp(s)^2}{\xi_\perp(0)^2}\left(1 + \frac{\xi_\parallel(s)^2}{\xi_\parallel(0)^2}\right)\rangle} \quad (3)$$

where $\xi_\perp(s)$ and $\xi_\parallel(s)$ are the perpendicular and parallel displacements of mass points with respect to the background field line because of interchange, and ρ is the mass density. Other variables and conventions are as defined above. The "e" subscript indicates that a term is evaluated in the equatorial plane, equivalent to setting $s = 0$ in the displacements. The first parenthetical term in the numerator is the entropy gradient evaluated at the equatorial plane,

while the second parenthetical term results from the Alfvenic-timescale pressure re-equilibration of the filament to the local background pressure. The pressure and flux tube volume are constants for a field line under the interchange approximation, so do not need subscripts. The Wolf2012 formula was compared to the Toffoletto et al. (2020) normal analysis, modified to include zero ionospheric conductance as well as the pure interchange result (equation 3). They found that tail-like field lines that cross the equatorial plane in the plasma sheet ($|x_e| > 15\ R_E$) are where the interchange results are most consistent with MHD ballooning normal mode analysis. One requirement for pure interchange is that the resulting pressure perturbation is constant along a field line, which is not generically the case for the more general MHD buoyancy modes.

This paper is a follow-up to the Toffoletto et al. (2022) paper, where we investigated the buoyancy properties inside a low entropy bubble. As before,w e use 3 approaches: (1) the Wolf2012 formula that depends on the entropy gradient, equation 1; (2) the MHD normal mode analysis described in Toffoletto et al. (2020) modified to use zero conductance ionospheric boundary conditions as in Toffoletto et al. (2022); (3) the pure interchange approached described in Toffoletto et al. (2022). The results are compared, including the predicted frequencies and associated normal mode and interchange perturbations. The rest of the paper describes the basic approach, including a brief description of the background equilibrium and how the low entropy perturbation was introduced. We show three examples and discuss the results.

2 Approach

2.1 Background Model of an Average Magnetosphere

For this study, we started with the same background field model as in Toffoletto et al. (2020, 2022), which consists of a Kp = 2 Tsyganenko (1989) model magnetic field and the pressure profile derived by combining a quiet curve from Lui et al. (1987) for $|x_e| < 8\ R_E$ and Spence et al. (1989) for $|x_e| > 8\ R_E$. The background field is relaxed to equilibrium in the *x*-*z* plane using a 2-D, high-resolution version of the friction code (Lemon et al., 2003). The density model is taken from the Kp = 2 Gallagher et al. (2000) model for $|x_e| < 8\ R_E$ merged smoothly to a Tsyganenko and Mukai (2003) model for $|x_e| > 10\ R_E$. The profile for this model along the *x*-axis is shown in Figure 1, which includes the pressure, magnetic field, and density model.

2.2 Local Entropy Depletion

To impose a change in entropy to simulate the presence of a bubble, we take the entropy profile from the background along the equatorial plane and impose an indentation (local entropy depletion) along the whole field line. This indentation is specified using four control points (x_1, x_2, x_3, x_4) and fitting three bicubic spline curves as illustrated in Figure 2. The spline fits are set between the control points $(x_i - x_{i+1})$, for $i = 1, 2, 3$. At the endpoints (x_1 and x_4) the value and derivative of $pV^{5/3}$ is matched to the original unmodified background, ensuring a smooth transition between regions. At the middle control points (x_2 and x_3) the value of $pV^{5/3}$and its derivative of the fitted curve is specified. In the cases shown below, the derivative is set to zero for simplicity at these locations. By field line tracing from each grid point in the 2D region to the intersection point

on the equatorial plane, any grid point that is magnetically connected to this region between the endpoints has its pressure modified to match the specified value of $pV^{5/3}$. This new configuration is then iterated to approximate force balance as before using a high-resolution version of a 2D friction code (Lemon et al., 2004), which results in a change in the entropy profile as the system relaxes to a new equilibrium now containing a localized entropy depletion. This equilibrium-setting process is important for the background to be suitable for linear stability analysis as the use of perturbation theory to perform an eigen-analysis presupposes an equilibrium background. In short, the relaxation procedure is necessary because the indentation procedure does not guarantee the preservation of pressure balance.

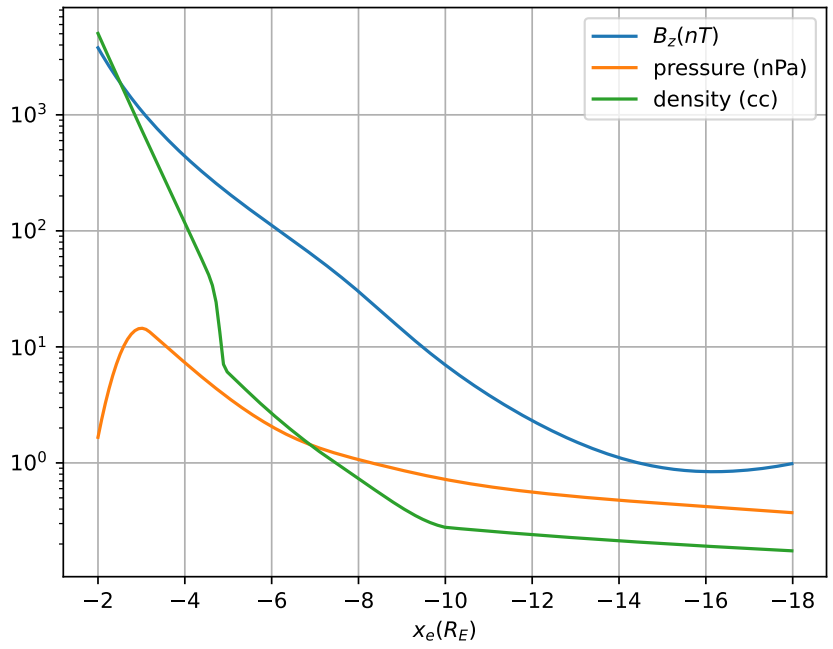

Figure 1: Plot of background magnetosphere model used, showing the pressure, B_z, and density along the tail axis in the equatorial plane as a function of equatorial distance. Note that the plasmapause at $-5\ R_E$ is incorporated in the density background.

Three cases are presented here: Case 1 represents a bubble near the Earth while Cases 2 and 3 represent a bubble further out in the plasma sheet. The parameters used are specified in Table 1.

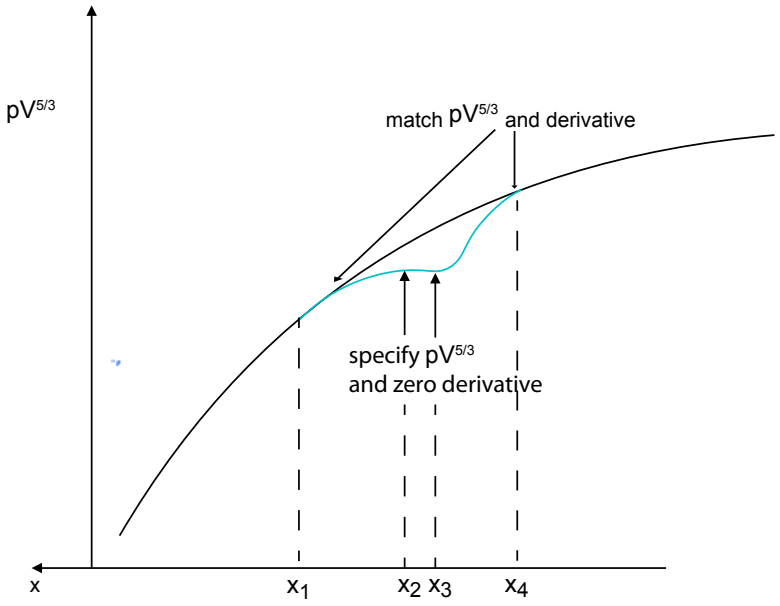

Figure 2: Sketch of the entropy profile along the equatorial plane along with the entropy-depleted region (in blue) showing the control points.

Table 1: Specification of entropy indentation geometry for three cases. Distances are in R_E and $pV^{5/3}$ in units of $nPa\ \left(\frac{R_E}{nT}\right)^{5/3}$.

Case	x_1	x_2	$pV^{5/3}(x_2)$	x_3	$pV^{5/3}(x_3)$	x_4
1	-4	-4.5	0.001	-5.5	0.0012	-6
2	-6	-6.5	0.008	-7.5	0.01	-8
3	-8	-8.5	0.04	-8.5	0.06	-10

Figures 3 through 5 show the resulting configuration before and after equilibration. The before plot includes the indentation but has not been restored to equilibriu, while the after plot shows the preservation of the indentation but is now at equilibrium. In all cases, the tailward portion of the bubble moves slightly earthward as the system relaxes to equilibrium, thus reducing the size of the entropy-depleted region. In Figures 4 and 5, which correspond to Case 2 and 3 respectively, the average plasma beta is higher, which results in a larger change in the magnetic field than for Case 1 and the resulting depleted region is smaller after equilibration. The entropy value at the control points x_2, and $x_3$were chosen so as have a slight positive tailward gradient and thus avoid unstable modes in this region, but this does not preclude unstable modes between the control points x_1 and x_2 at the Earthward

end of the bubble. We do not include cases where the bubble was placed further tailward, as it resulted in a dramatic reconfiguration of the tail during the equilibration process and a collapse of the bubble. As can be seen in Figure 1, the background magnetic field had a B_z minimum centered at around $x_e = -16\ R_E$, and the resulting magnetic field with a tailward bubble further reduced the minimum.

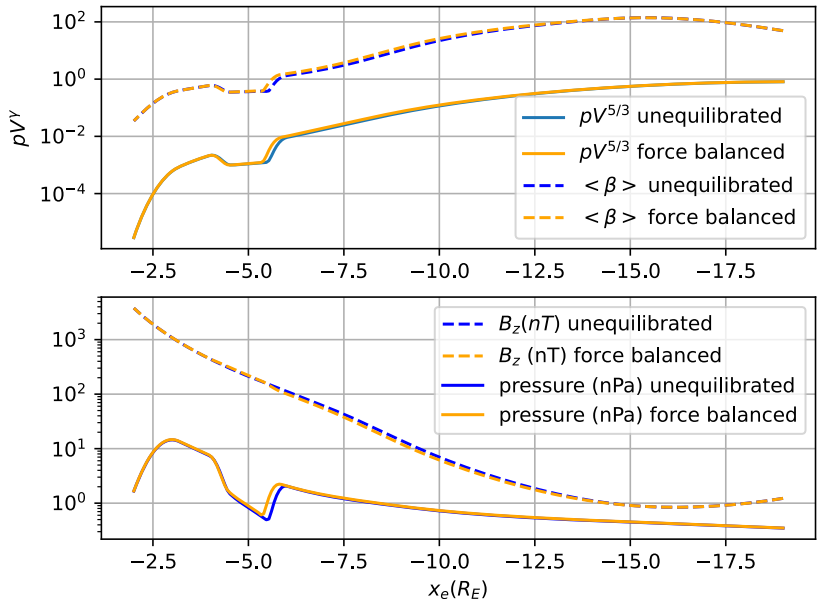

Figure 3: Top panel shows $pV^{\frac{5}{3}}$ in units of $nPa\left(\frac{R_E}{nT}\right)^{\frac{5}{3}}$ and field line average plasma beta (equation 2) before and after equilibration for Case 1 where the indentation is placed between $x_e = -4R_E$ and $-6\ R_E$. The bottom panel shows B_z(in nT) and pressure (in nPa).

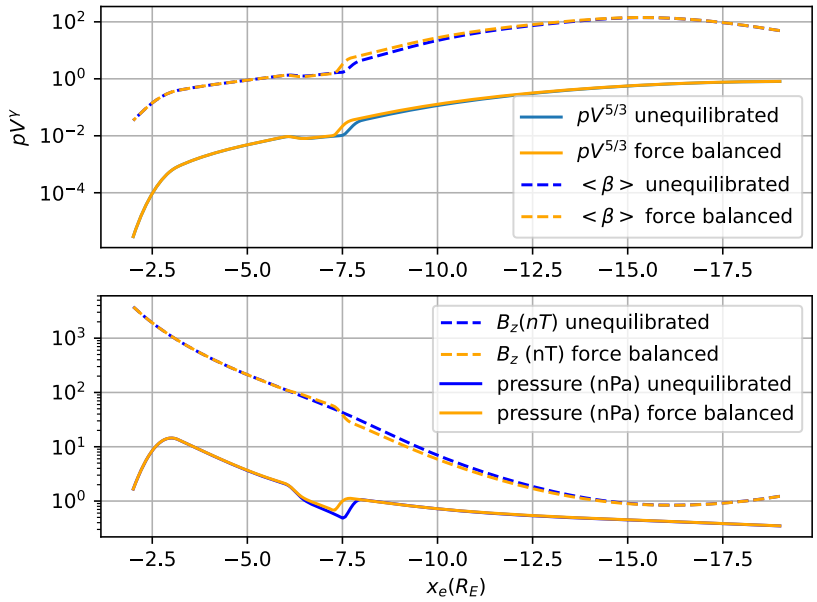

Figure 4: Same format as Figure 3 for Case 2 where the indentation is placed between $x_e = -6\ R_E$ and $-8\ R_E$.

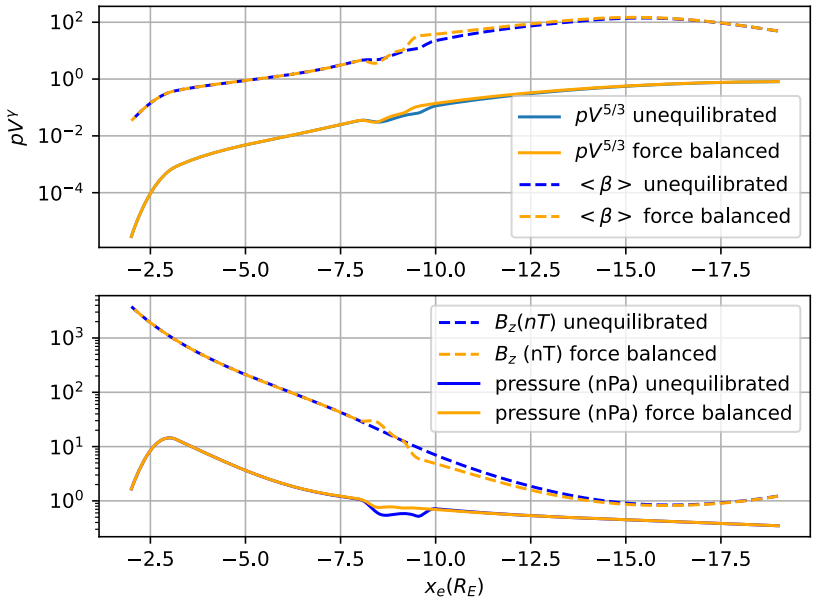

Figure 5: Same format as Figure 3 for Case 3 where the indentation is placed between $x_e = -8\ R_E$and $-10\ R_E$. Note the larger change in the magnetic field after equilibrium than the other two cases.

3.0 Results

Equatorial Footprint Location (R_E)	Background Frequency (Hz) from MHD Normal Mode	Bubble Frequency (Hz) from MHD Normal Mode	Background Pressure Standard Deviation (nPa)	Bubble Pressure Standard Deviation (nPa)	MHD Mode
-6.0	0.0105	0.0150	0.981	0.854	
-5.5	0.0107	0.0087	1.362	0.895	slow mode
-5.2	0.0109	0.0027	1.711	0.133	pure interchange
-5.0	0.0112	0.0033	2.026	0.063	pure interchange
-4.8	0.0082	0.0025	2.427	0.092	pure interchange
-4.6	0.0057	0.0010	2.934	0.149	pure interchange
-4.4	0.0053	0.0060i	3.674	0.856	unstable
-4.2	0.0050	0.0081i	4.390	2.532	unstable
-4.0	0.0048	0.0035	5.428	2.225	

Table 2: Summary of the results for Case 1. Column 1 shows the sampling location in the equatorial plane, the second and third column frequency of the normal mode oscillation from the background and the bubble frequency respectively, the third and fourth column show the standard deviation of the isotropic pressure perturbation for the background and bubble, and the fifth column is the mode produced by the MHD normal mode analysis.

3.1 Case 1

The first case is the indentation is the closest to the Earth of all three cases. Table 2 lists the results on some sampled field lines inside the bubble. The solid line in the top panel of Figure 6 is a plot of the entropy profile for both the unperturbed background (blue) and the indented profile (orange), and the dashed line is the corresponding flux tube volume averaged plasma beta (see equation 2 for our definition of flux tube volume average). Note that the profiles are slightly different even outside the control region because of the equilibration process. Also, the values of the entropy are slightly different from the specified values for the same reason. The second panel of Figure 6 shows the *z*-component of the magnetic field and pressure along the *x*-axis (in the equatorial plane) for both the background field and the bubble indentation. The third panel of Figure 6 shows the computed buoyancy frequencies for the background field and bubbles using three different techniques, the curves labeled MHD correspond to the normal mode calculation; the curves labeled "Wolf" are from the Wolf2012 approximate plasma sheet while the curves labeled "PI" are from the pure interchange calculation (equation 3). These frequencies are scaled to the background density profile shown in Figure 1, as described above and in Toffoletto et al. (2020). Since the eigenvalues can in principle be imaginary, both real and imaginary parts are included, where the imaginary components are shown as a dashed line with a shaded background and indicate regions of instability. The change in frequency at around $x_e = -5\ R_E$ corresponds to the plasmapause location in the Gallagher (2000) model.

For this case, Figure 8 and Table 2 shows that there is an overlap of the MHD normal modes and the pure interchange results at the locations $x_e = -4.6, -4.8, -5.0,$

and $-5.2\ R_E$. In Figure 9 and Table 2 the normalized pressure perturbation from the MHD normal mode analysis as a function of distance s along the field line (from the equator) for the background field is a solid line and a dashed line for Case 1 bubble. The standard deviation of pressure along the field line (in nPa) for the background and bubble is also shown. For this case, the pressure perturbation at $x_e = -4.6, -4.8, -5.0$ and $-5.2\ R_E$ is approximately constant along the field line, as can be seen in the reduction in the standard deviation of the pressure perturbation compared to the background. This is consistent with the modes at these locations being pure interchange. All displacements are normalized by the maximum displacement of all the modes (Toffoletto et al. 2020).

The computed frequency at these locations is much lower than the ones obtained in the background case with no bubble, and all three approaches give quite consistent results at these locations. This would imply that the buoyancy frequencies inside a low entropy bubble with a small entropy gradient would be small and closer to the values one would expect for the plasmasheet rather than the inner magnetosphere. For $x_e = -4.2$ and $-4.4\ R_E$ the solution is imaginary, indicating instability. The large value of the frequency tailward of the region of instability (between $x_e = -5$ and $-6\ R_E$) is a result of a large negative gradient in $pV^{5/3}$ as its value returns to the background value outside the bubble. The MHD normal modes for $x_e = -5.5\ R_E$ indicate slow mode solutions as the parallel displacement is much larger than the perpendicular displacement. For this location, the MHD normal mode predicts a much lower frequency than the pure interchange and Wolf2012 result.

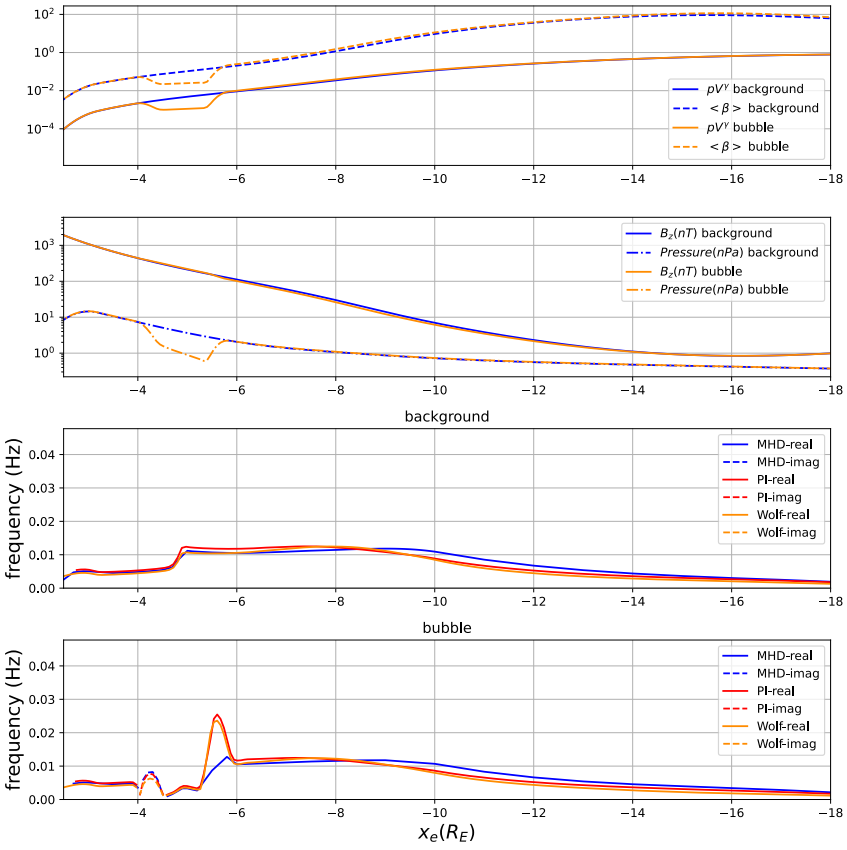

283 Figure 6: The is the result for Case 1. The solid line in the top panel shows $pV^{\frac{5}{3}}$and the
284 dashed line is the field line average plasma beta. for both the background and perturbed
285 configuration. The units for $pV^{5/3}$are $nPa\ (R_E/nT)^{5/3}$. The second panel shows the
286 magnetic field (B_z) in nT and pressure in nPa. The third panel shows the computed
287 frequencies (in Hz) for the unperturbed field using the MHD normal mode approach (blue),
288 pure interchange (red) and the Wolf2012 formula (orange). The solid lines are for real
289 values, the dashed lines imaginary. In this case, all frequencies are real. The bottom panel

shows the computed frequencies for the perturbed background, showing a shaded region of imaginary frequencies between $x_e = -4.1$ and $-4.4\ R_E$.

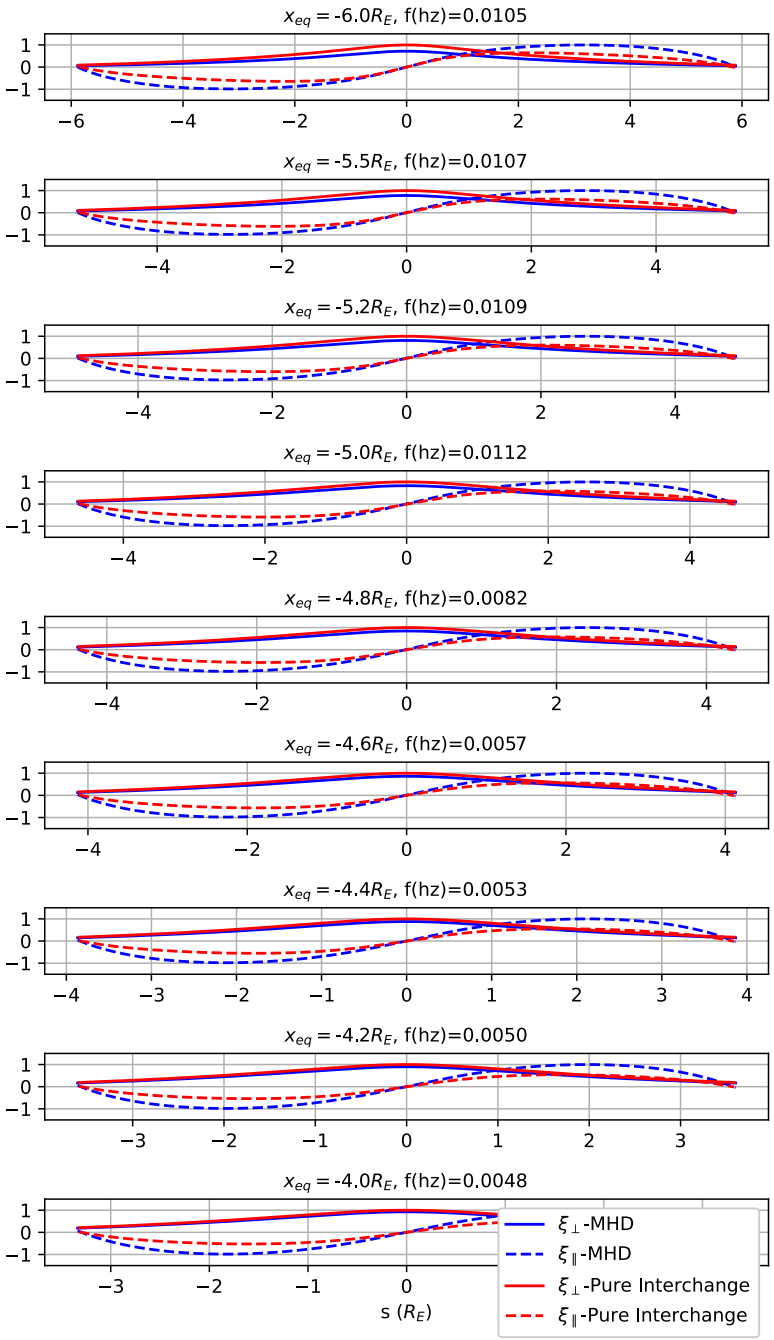

Figure 7: Comparison of wave modes from the MHD normal mode (blue line) and classic interchange analysis (red line) for the background field as a function of distance s along the field line from the equator. The solid curves represent the perpendicular displacement and the dashed line is the parallel displacement. The associated MHD normal mode frequencies

297 are also shown. All results are normalized to the maximum displacement of the largest
298 mode.

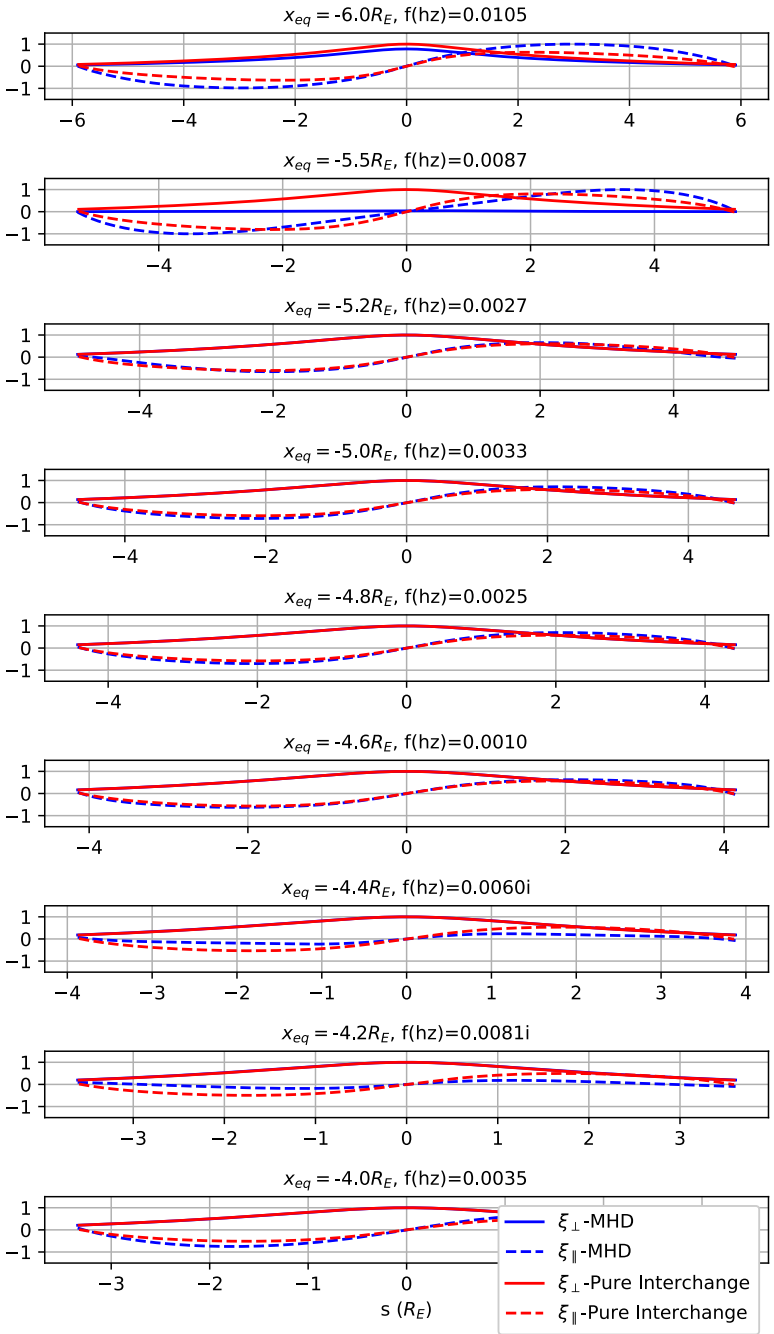

299

300 Figure 8: Same format as Figure 7 for the bubble indentation field for Case 1. Note the
301 overlap of the modes for $x_e = -4.6, -4.8, -5.0$ and $-5.2\ R_E$. Note that for $x_e = -4.2$
302 and $-4.4\ R_E$ the solution is imaginary, indicating instability. The MHD normal modes for
303 $x_e = -5.5\ R_E$ indicate slow mode solutions, as the parallel displacement is much larger than
304 the perpendicular displacement.

305

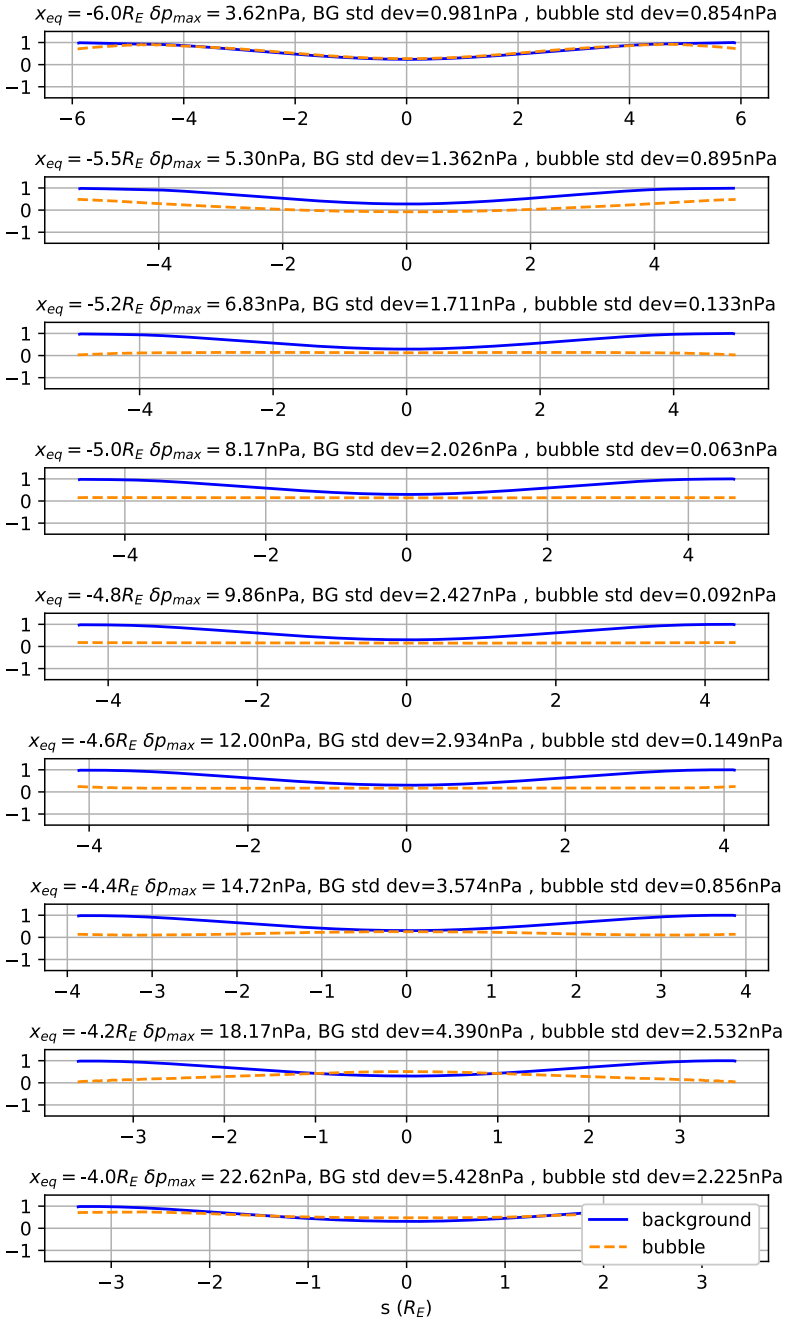

306

307 Figure 9: Pressure normalized perturbation from the MHD normal mode analysis as a
308 function of distance s along the field line (from the equator) for the background field is a
309 solid line and a dashed line for Case 1 bubble. The standard deviation of pressure along the
310 field line (in nPa) for the background and bubble is also shown. For this case, the pressure
311 perturbation at $x_e = -4.6, -4.8, -5.0$ and $-5.2\ R_E$ is approximately constant along the
312 field line, as can be seen in the reduction in the standard deviation of the pressure
313 perturbation compared to the background.

314

3.2 Case 2

The results for Case 2 are shown in Figure 10 and summarized in Table 3. The ordinary (unindented) background and the bubble oscillation frequencies are quite different and vary noticeably between -6 and $-8\ R_E$. Note that the eigenvalues are only purely real or imaginary as there is no dissipation in the system. In the case of the ordinary background fields, there are only real eigenvalues, indicating a stable equilibrium with no dissipation. The bottom panel shows the corresponding results for the bubble indentation. For this case, there is a shaded region of imaginary eigenvalues between approximately $x_e = -6.1$ and $-6.3\ R_E$ where the gradient in $pV^{5/3}$ is positive (decreasing away from the Earth), as the chosen entropy value is set to allow a change in gradient at the earthward edge of the imposed bubble. The large value of the frequency tailward of the region of instability (between $x_e = -7$ and $-8\ R_E$) is a result of a large negative gradient in $pV^{5/3}$ as its value returns to the background value outside the bubble. No such increase in frequency is seen in the MHD normal mode result. The reason for the difference can be seen in Figures 11 and 12, which plot the normalized modes for both the pure interchange (solid line) and the MHD normal mode calculation. As before, the normalization is chosen relative to the maximum of all the modes (see Toffoletto et al., 2020 for a discussion of the normalization). Figure 11 is from the background field and Figure 12 for the imposed bubble indentation. In Figure 12, at $x_e = -7.5\ R_E$, which corresponds to the location where there is a jump in the frequency in Figure 10, the parallel displacement for the MHD is larger than the perpendicular displacement, which is what would be expected from an MHD slow mode. These results suggest that to remain compatible with pure interchange assumptions at this location a much higher frequency is needed, while the MHD solution produces a lower frequency but as a slow mode. In other words, the assumptions underlying the pure interchange calculation prevent the slow mode observed in the MHD results from showing up. In addition, as can be seen in Figure 12, at $x_e = -6.5\ R_E$ the pure interchange solution closely resembles the MHD solution, which implies the MHD solution is closer to being a pure interchange mode at this location. This can be confirmed by the pressure perturbation, which is shown in Figure 13, which shows a reduction in the standard deviation of the pressure along the field line from 0.759 to 0.154 nPa. We see similar behavior at $x_e = -7.2\ R_E$. Unstable modes are also shown in Figure 13 at $x_e = -6.0$ and $-6.2\ R_E$. At the sampling locations at $x_e = -6.4, -6.5$ and $-7.2\ R_E$ shows a good overlap between the MHD normal mode and pure interchange and the pressure perturbation is approximately constant along the field lines. Outside the bubble region, tailward of $x_e = -8\ R_E$ and earthward of $x_e = -6\ R_E$, the solutions are close to the background field; i.e., the frequency curves in the middle and lower panels of Figures 11 and 12 are almost identical. Any difference between them is due to the equilibration of the tail after the bubble indentation was introduced.

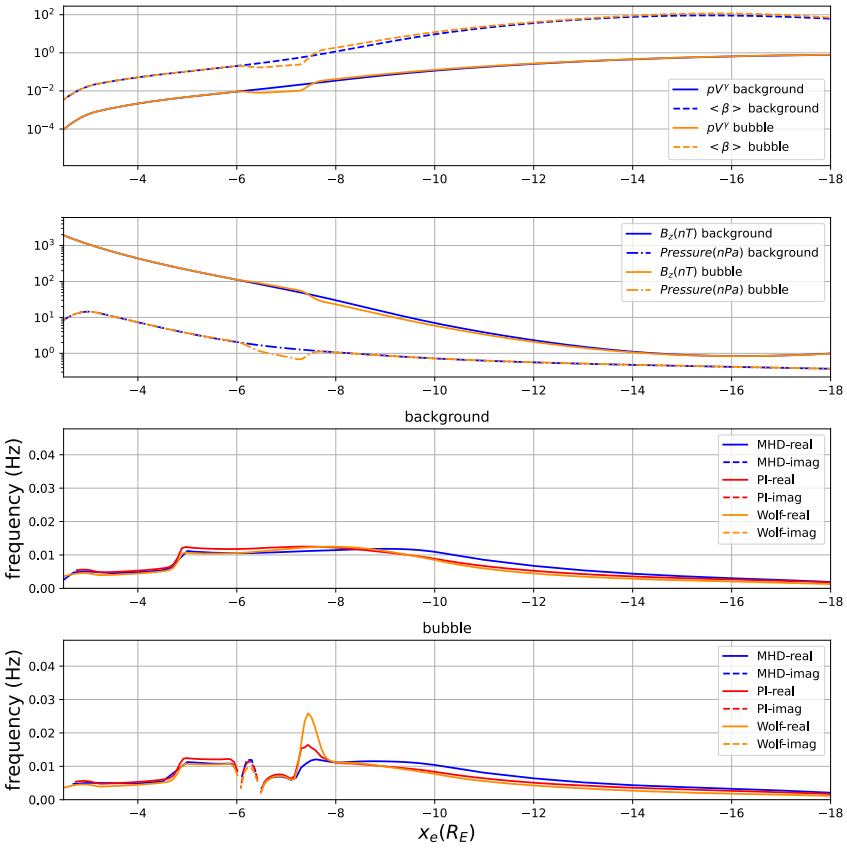

Figure 10: This shows the results for Case 2, the solid line in the top panel shows $pV^{\frac{5}{3}}$and the dashed line is the field line average plasma beta. for both the background and perturbed configuration. The units for $pV^{5/3}$are $nPa\ \left(\frac{R_E}{nT}\right)^{5/3}$. The second panel shows the magnetic field (B_z) in nT and pressure in nPa. The third panel shows the computed frequencies (in Hz) for the unperturbed field using the MHD normal mode approach (blue), pure interchange (red) and the Wolf2012 formula (orange). The solid lines are for real solutions, the dashed lines are imaginary solutions. In this case, all frequencies are real. The bottom panel shows the computed frequencies for the perturbed background, showing a shaded region of imaginary frequencies between $x_e = -6.0$ and $-6.2\ R_E$.

Equatorial Footprint Location (R_E)	Background Frequency (Hz) from MHD Normal Mode	Bubble Frequency (Hz) from MHD Normal Mode	Background Pressure Standard Deviation (nPa)	Bubble Pressure Standard Deviation (nPa)	MHD Mode
-9.0	0.0118	0.0150	0.289	0.272	
-8.0	0.0114	0.0087	0.414	0.370	
-7.5	0.0112	0.0027	0.499	0.501	slow mode

-7.2	0.0110	0.0033	0.560	0.119	pure interchange
-6.5	0.0107	0.0025	0.759	0.154	pure interchange
-6.4	0.0106	0.0010	0.792	0.217	pure interchange
-6.2	0.0106	0.0060i	0.877	0.627	unstable
-6.0	0.0105	0.0081i	0.981	0.578	unstable
-5.0	0.0122	0.0035	2.026	2.049	

Table 3: Summary of the results for Case 2. Column 1 shows the sampling location in the equatorial plane, the second and third column frequency of the normal mode oscillation from the background and the bubble frequency respectively, the third and fourth column show the standard deviation of the pressure perturbation for the background and bubble, and the fifth column is the mode produced by the MHD normal mode analysis.

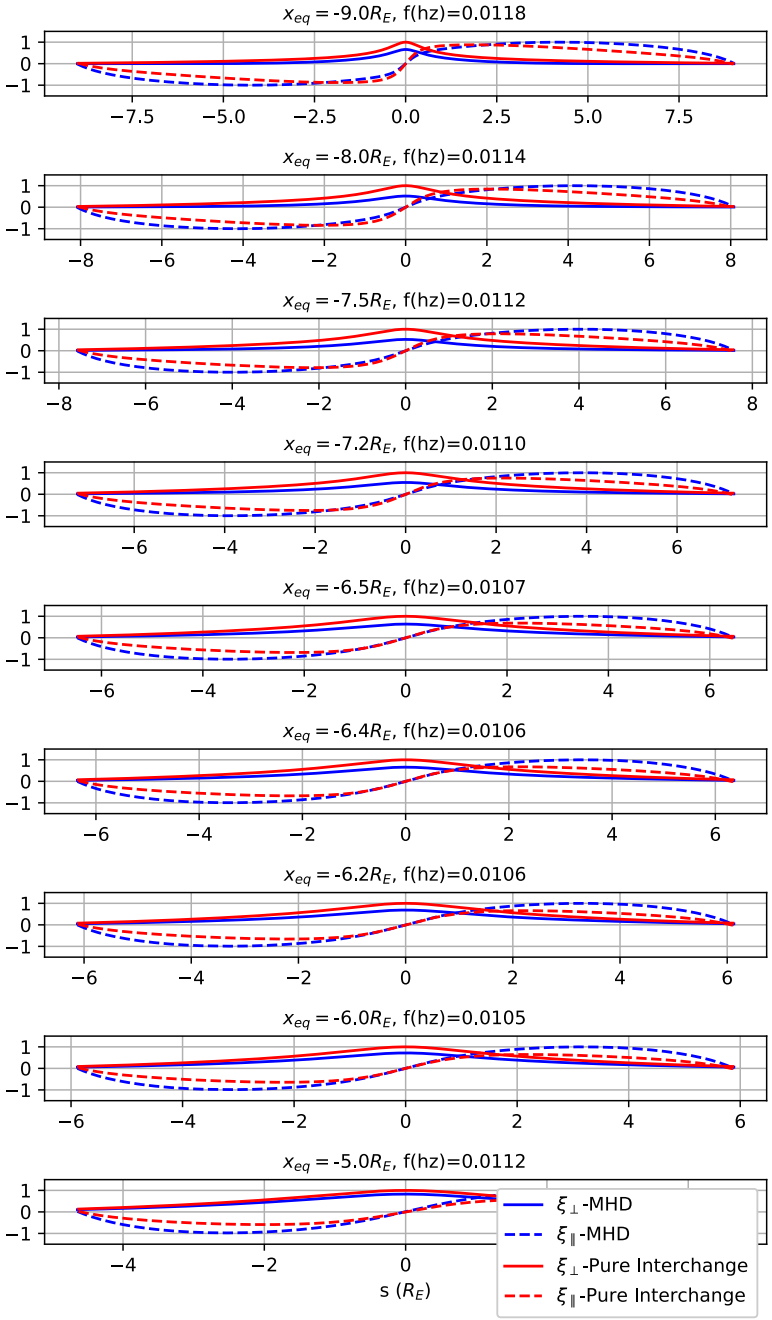

Figure 11: Comparison of wave modes from the MHD normal mode pure (blue line) and interchange analysis (red line) for the background field as a function of distance s along the field line from the equator. The solid curves represent the perpendicular displacement and the dashed line is the parallel displacement. The associated MHD normal mode frequencies are also shown.

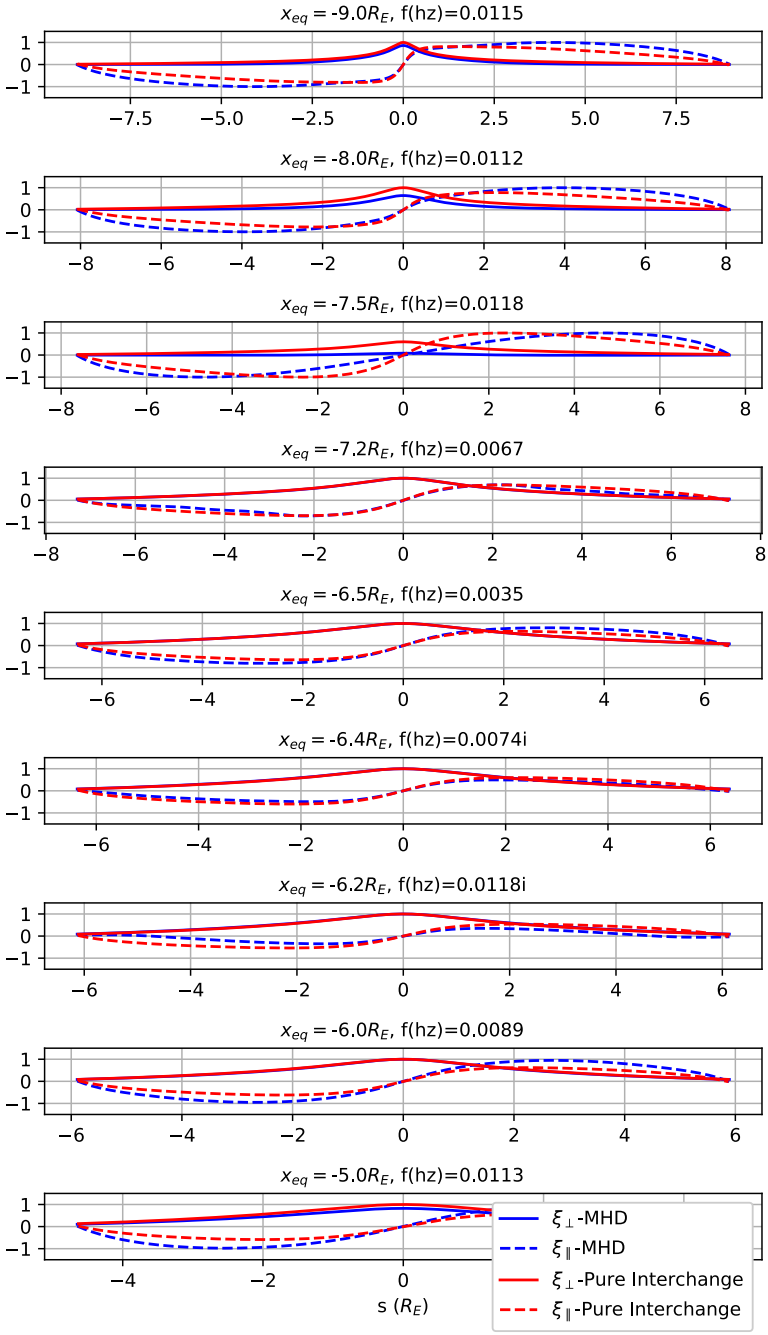

Figure 12: Same format as Figure 7 for the bubble indentation field for Case 2. Note the overlap of the modes for $x_e = -6.4, -6.5$ and $-7.2\ R_E$. Note that for $x_e = -6.0$ and $-6.2\ R_E$ the solution is imaginary, indicating instability. At $x_e = -7.5\ R_E$ we see slow mode waves in the MHD normal mode solution, where motion is dominated by parallel displacement.

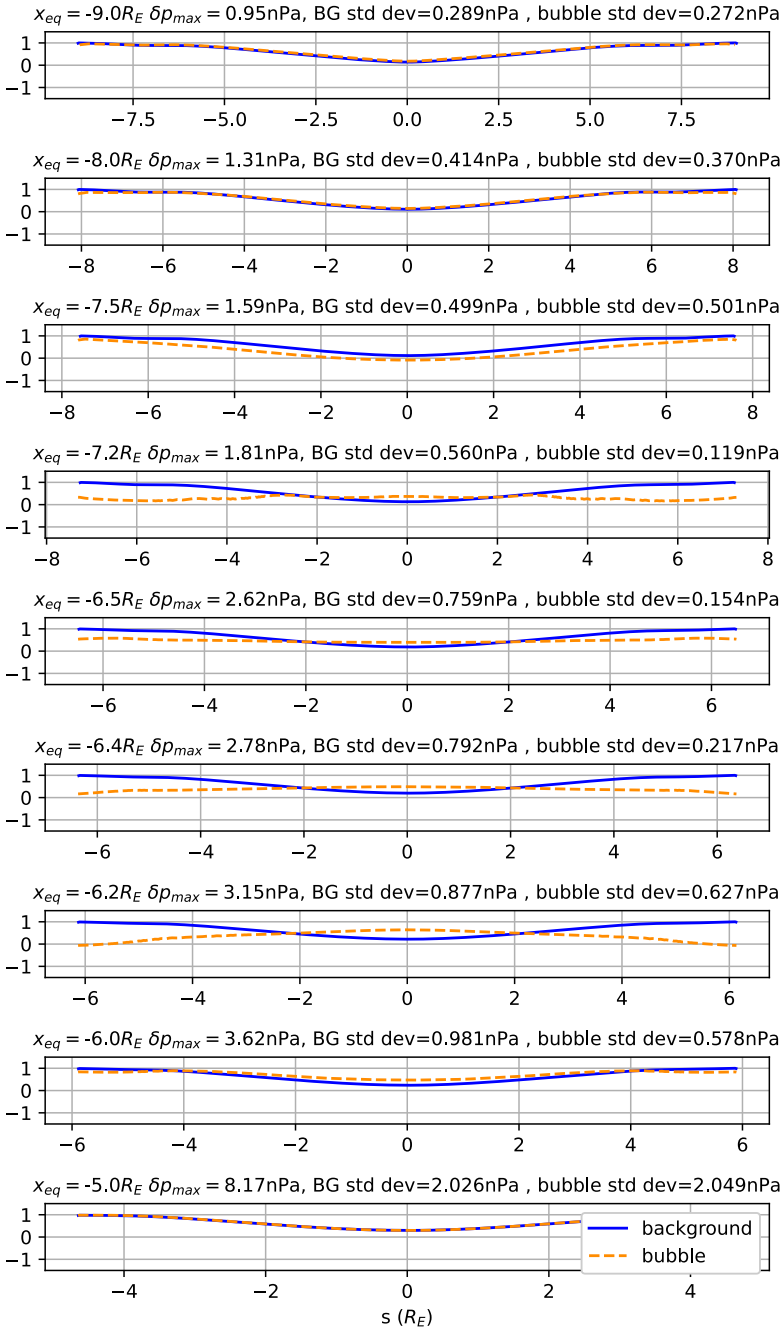

Figure 13: Pressure normalized perturbation from the MHD normal mode analysis as a function of distance s along the field line (from the equator) for the background field is a solid line and a dashed line for Case 2 bubble. The standard deviation of pressure along the field line (in nPa) for the background and bubble is also shown.

3.3 Case 3

For this case, the indentation corresponds to an entropy bubble that is further out in the plasma sheet. Figure 14 shows the configuration and resulting buoyancy frequency results for this case and is summarized in Table 4. The bubble was set in the range $x_e = -8$ to $-10\ R_E$. The perturbation in $pV^{5/3}$ was set by specifying the pressure, but the resulting equilibration relaxes the pressure closer to the background while changing the magnetic field. Such a resetting of the pressure was not seen in Case 1, likely because the background plasma beta is lower in Case 1. These results indicated instability on the tailward portion of the bubble front around $x_e = -8.2\ R_E$ where the derivative of $pV^{5/3}$ reverses sign. The MHD normal mode results most closely resemble the pure interchange results for a field line that crosses the equatorial plane at $x_e = -8.4\ R_E$. This can be seen in the overlap of the modes in Figure 15, as well as the pressure perturbation plot in Figure 16, although the pressure for this case is only approximately constant along the field line. As in Case 1, there is a difference in the predicted modes at around $x_e = -8.7$ and $-9.0\ R_E$, the Wolf2012 (equation 1) formula predicts a higher frequency than the MHD normal mode, while the pure interchange frequencies (equation 3) are closer to the MHD result, and both are closer to the background result (e.g., Figures 15 and 16, $x_e = -10\ R_E$). The MHD normal mode results are, as in Case 1, slow mode waves where the parallel displacement is significantly larger than the perpendicular displacement, as can be seen in Figure 16. The pressure perturbation is approximately constant for a field line that crosses the equatorial plane at $x = -8.4\ R_E$, with a standard deviation of 0.086 nPa, compared to the unperturbed value of 0.359 nPa.

I

Equatorial Footprint Location (R_E)	Background Frequency (Hz) from MHD Normal Mode	Bubble Frequency (Hz) from MHD Normal Mode	Background Pressure Standard Deviation (nPa)	Bubble Pressure Standard Deviation (nPa)	MHD Mode
-11.0	0.0085	0.0074	0.060	0.028	
-10.0	0.0109	0.0096	0.166	0.035	
-9.5	0.0116	0.0123	0.239	0.264	
-9.0	0.0118	0.0115	0.289	0.266	
-8.7	0.0118	0.0120	0.322	0.345	slow mode
-8.4	0.0117	0.0028	0.359	0.086	pure interchange
-8.2	0.0116	0.0154i	0.385	0.303	unstable
-8.0	0.0114	0.0094	0.414	0.281	
-7.0	0.0109	0.0110	0.606	0.619	

Table 4: Summary of the results for Case 3. Column 1 shows the sampling location in the equatorial plane, the second and third column frequency of the normal mode oscillation from the background and the bubble frequency respectively, the third and fourth column

421 show the standard deviation of the pressure perturbation for the background and bubble, and
422 the fifth column is the mode produced by the MHD normal mode analysis.

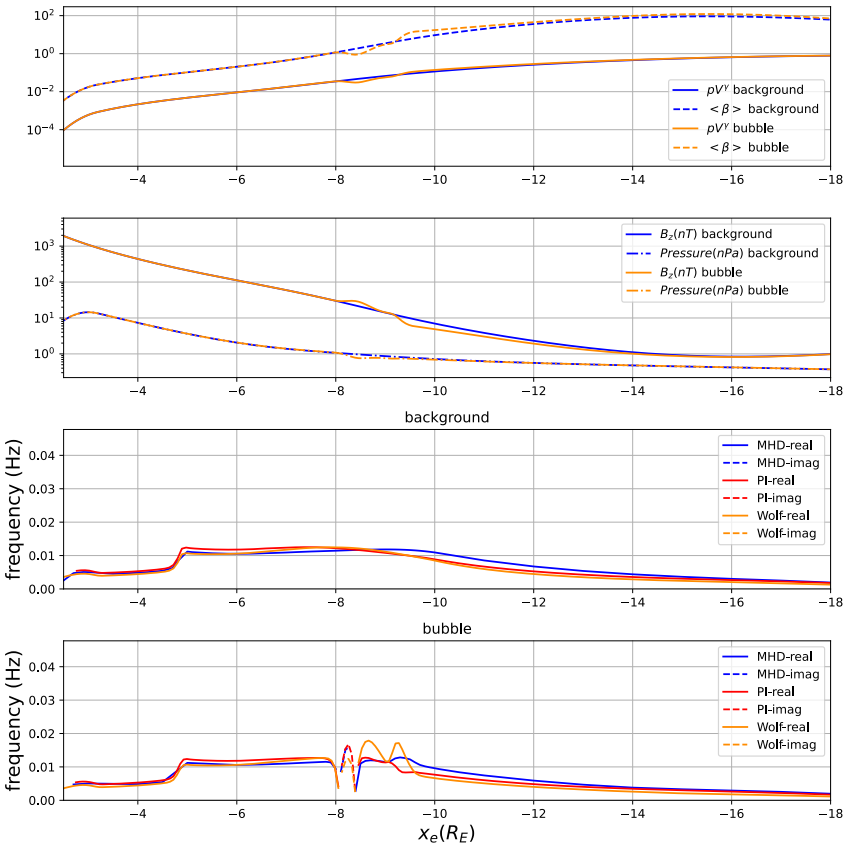

423

Figure 14: Same format as Figure 6 for Case 3. The shaded region indicates where the modes are unstable.

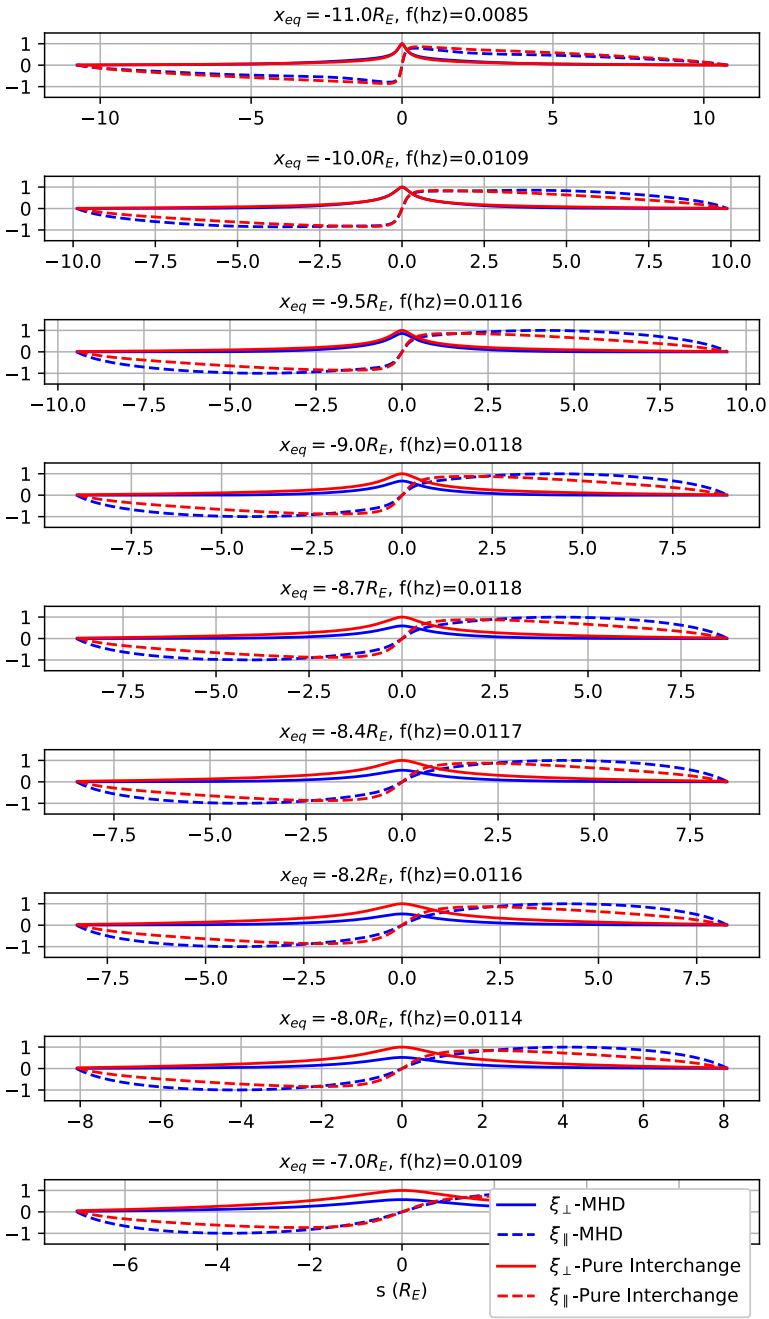

427 Figure 15: Same format as in Figure 7 for the background field for comparison for Case 3.

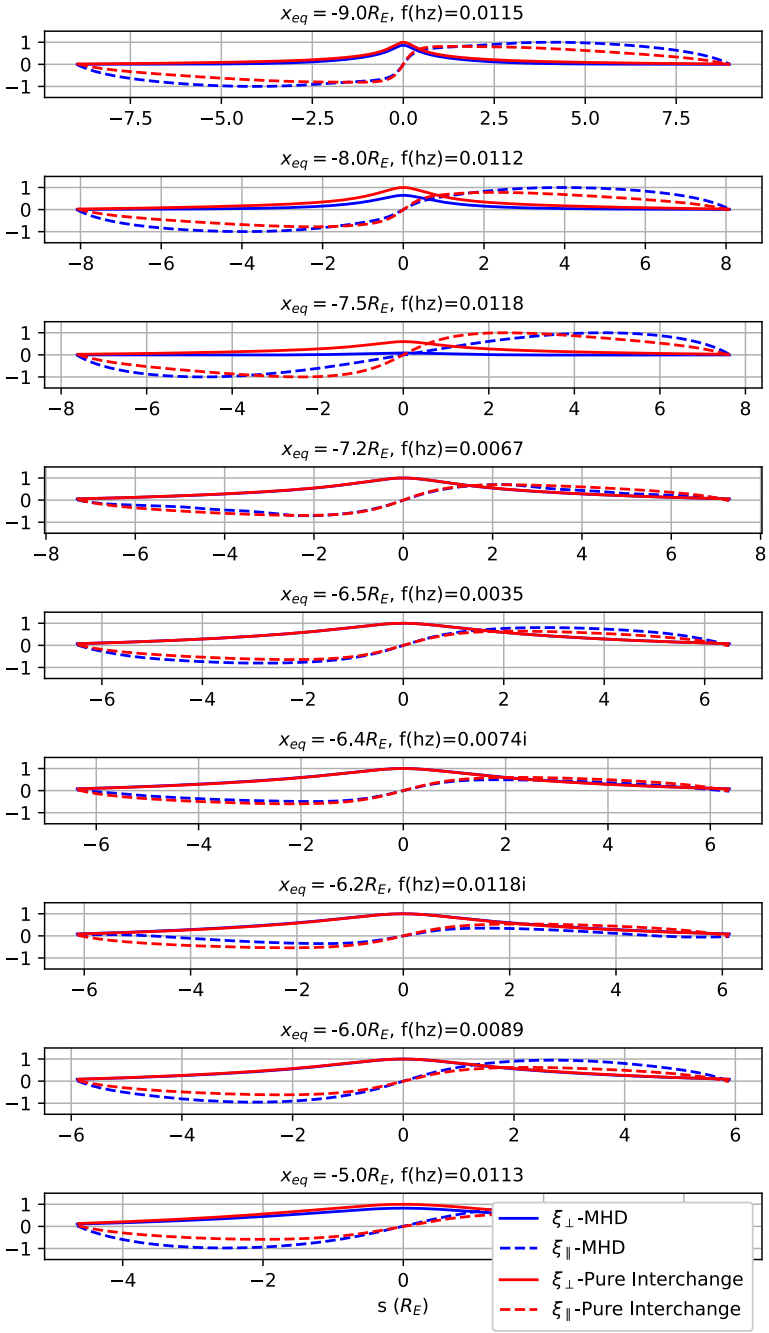

428

429 Figure 16: Same as Figure 8 for Case 3.. Note the overlap in modes for the field line that
430 crosses the equatorial plane at $x_e = -6.5$ and $-7.2\ R_E$, $x_e = -6.2$ and $-6.4\ R_E$ are
431 unstable modes.
432

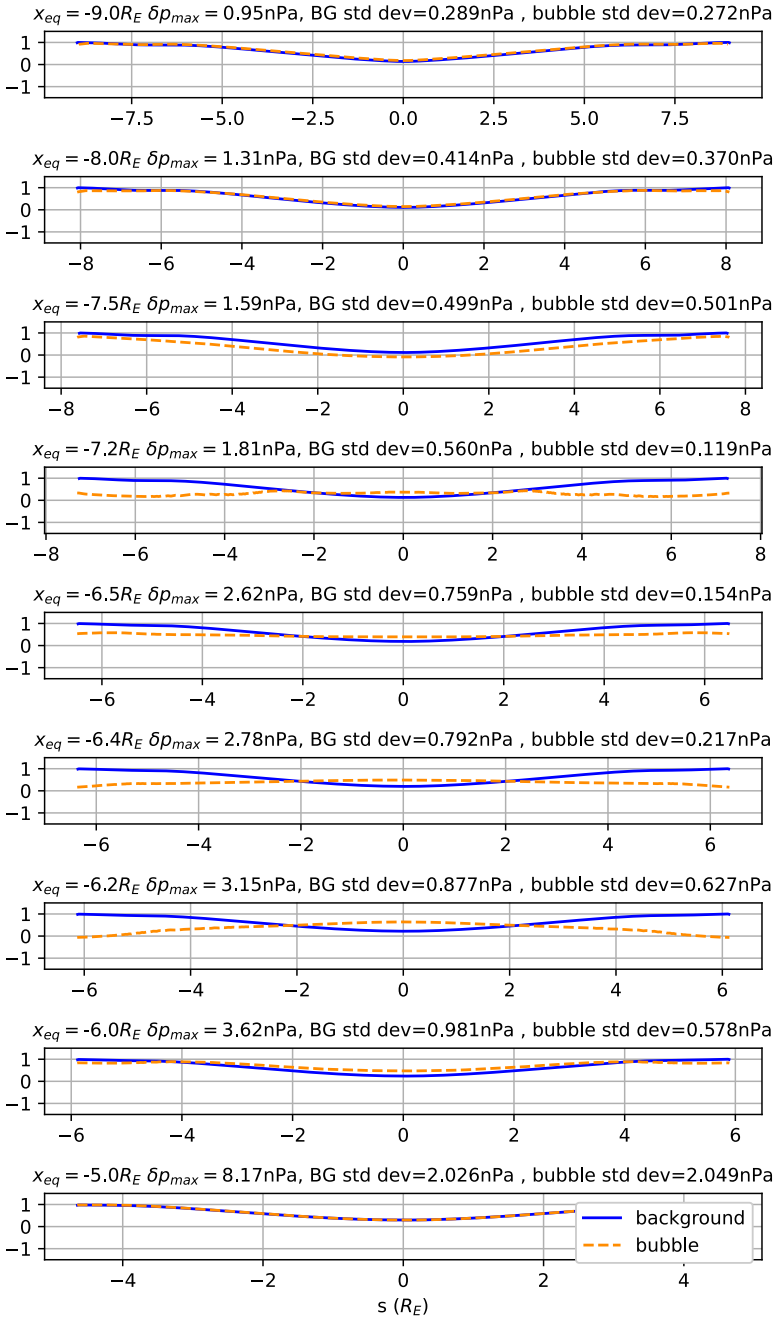

Figure 17: Same as Figure 9 for the background for comparison for Case 3. Note the pressure is approximately constant along the field lines that have crossing points at $x_e = -6.5\ R_E$, and are approximately consistent with these modes being an interchange mode.

4.0 Discussion

The thin filament approximation, while limited in many ways, has proven to be a useful approach to looking at the properties and motion of entropy-depleted field lines in a background medium. The approach follows a one-dimensional field line, neglecting the

motion of the field lines transverse to the noon-midnight meridional (*x*-*z*) plane. However, for the interchange of two field lines to occur, they must move past one another in such a way that both cannot remain in-plane. In addition, the MHD thin filament code neglects feedback from the background and any other filament while this coupling is explicitly included in the interchange derivation. The coupling to the other filaments should be included to properly compare some features of the MHD thin filament model to the classic interchange model. This work is a follow-up to the previous study looking at buoyancy modes where the entropy has been modified relative to the ordinary background to include a bubble, all within the framework of the MHD thin filament approximation (Chen and Wolf, 1999; Wolf et al. 2012). After imposing entropy modifications at three locations on the nightside magnetosphere, we used three different approaches to infer the properties and frequencies of buoyancy modes within these entropy-depleted regions. Our methodology (average background, indentation-relaxation, eigen-analysis) presupposes that the bubble can be treated quasi-statically on the timescales of the oscillations. The three approaches used in this study are:

1. MHD normal mode calculation, the basic procedure is described in Toffoletto et al. (2020) except that the ionospheric boundary condition is replaced with a zero conductance, to be consistent with the interchange assumption. The modifications to the boundary conditions are described in Toffoletto et al. (2022).
2. Pure interchange (equation 3) as described by Toffoletto et al. (2022), used an energy argument to deduce the modes and frequencies that one would expect when the assumptions of the classic interchange theory is applied. This assumption entails that both the background pressure and associated pressure perturbation that arises from interchange is constant along a field line.
3. The Wolf2012 (equation 1) formula is based on simplifying assumptions of interchange in a tail-like background equilibrium magnetic field.

Three cases are examined:

Case 1 involves an entropy depletion (bubble) centered at $x = -7$ R_E where it is found that the frequency of the interchange mode is much lower than a typical field line would be than a background field line at that location. Some of field lines resembled pure interchange modes, as shown in Figure 8 and Table 2a for the field line crossing the equatorial plane at $x_e = -6.4$ and -6.5 R_E, where the pure interchange mode and the MHD normal mode overlap quite closely and the pressure perturbation from the MHD result is approximately constant along the field line. The analysis also reveals the existence of unstable modes between $x_e = -6.4$ to -7.2 R_E where the entropy gradient changes sign to decreasing tailward. All three approaches predict a very similar buoyancy frequency with the normal mode and interchange analysis having the closest agreement. It is surprising how well the Wolf2012 estimate works given that it is an approximate formula that was developed for a tail-like background. On the tailward edge of the bubble, the MHD normal mode results disagree with the pure interchange and the Wolf2012 estimate. The MHD result predicts slow mode waves ($x_e = -7.5$ R_E in Figure 8 and Table 2) with lower frequencies, while the pure interchange and the Wolf2012 formula predict a larger frequency. Since the MHD result is more general and does not restrict itself to any interchange assumptions, one would expect that this result is likely more physically

reasonable. Nevertheless, except for this tailward region of the bubble, it is remarkable how well the three approaches agree, in particular regarding the frequencies.

Case 2 represents a bubble that is further out in the tail and resulted in a small region of unstable modes as in Case 1 and also lower frequencies inside the bubble, however, the modes are less like pure interchange modes than in Case 1. In both cases, we find that the buoyancy frequencies are lower in the bubble, and on the field lines that crosses the equator at $x_e = -6.4, -6.5$, and $-7.2\ R_E$ the MHD result resembles pure interchange modes where pressure perturbation is approximately constant along the field line (see Figure 13, Table 3). We also find that on the tailward portion of the bubble, the buoyancy mode results disagree, the MHD normal mode solution finds a lower frequency solution than pure interchange and Wolf2012 and produces a slow mode wave with motion dominated by the parallel displacements of mass points lining the filament. Nevertheless, it is surprising how well the frequencies arrived at using very different methods agree given that the simplifying assumptions implicit in the MHD thin filament code.

Finally, Case 3 is for a bubble even further out in the tail. The indentation-relaxation procedure results in a larger disruption of the tail equilibrium outside the indentation region that produces a deeper B_z minimum in the tail, likely due to the greater plasma β on stretched field lines. We see a region of slow mode dominated behavior in the MHD solution tailward of the instability region as in the other cases. A smaller region of obvious pure interchange modes within the bubble are seen in this case, as shown for the field line the crosses the equatorial plane at $x_e = -8.4\ R_E$.

Now, we discuss our implicit interpretation of disagreement between the two methods under consideration (MHD vs. pure interchange). In some sense, the pure interchange approach is a "more constrained" approach in virtue of the additional assumption of pressure constancy along a field line. For this reason, we interpret a disagreement between the results of the interchange approach and the MHD approach as a violation of the additional assumptions behind pure interchange. In short, we imply that the ideal MHD is closer to ground truth. However, there is reason to approach such an assumption with caution. It may be that the conditions of the magnetotail are such as to violate MHD while producing kinetic effects that substantiate a pure interchange treatment.

MHD treatments presuppose that interactions between the plasma and electromagnetic fields occurs locally, which requires that the frequencies be much slower than the gyrofrequency and wavelengths much later than gyroradius. However, when the magnetosphere is stressed, the near Earth plasma sheet (NEPS) undergoes thinning, the plasma β increases and the local field line curvature increases. When the field line curvature becomes comparable to the local gyroradius, the ion orbits become stochastic, undergoing stochastic (non-adiabatic) pitch-angle scattering each time it crosses the equatorial plane. This violate bounce invariance, since its motion is largely adiabatic away from the equatorial plane, meaning that one should in such cases perform a bounce-averaging. These arguments are considered in great detail in Hurricane (1994 a,b), where a linear kinetic Vlasov theory for ballooning-interchange modes is developed to capture NEPS dynamics. The paper also provides support for performing flux tube (field line) averaging (bounce averaging and pitch angle averaging) of drift frequencies in cases of high stochasticity, since the individual particles will explore most of the flux tube volume in a small number of bounces.

The main implication of these points is that it may be more realistic in the NEPS to entertain the validity of the interchange assumption over MHD, which allows greater flexibility in the pressure adjustments. In short, where the results of the interchange analysis deviate from the MHD analysis above, it is not obvious that the MHD results are the more trustworthy. Perhaps we should remain open to the question of which conditions are more well-satisfied in the NEPS. For example, we were unable to find any observational data pertaining to slow modes towards the tailward region of flow bursts. Observational data could either find such modes near the bubble's tailward edge or fail to, in which case some empirical support would be provided for the greater applicability of either the MHD approach or the interchange approach, respectively.

5.0 Conclusion

Using empirically based magnetic field and pressure models, the entropy $pV^{5/3}$ is generally found to be a smooth background function of x_e, where x_e is the distance in the equatorial plane and increases sunward. Additionally, $\partial(pV^{5/3})/\partial x_e$ is normally negative for $x_e < 0$. In the present paper, we let $\partial(pV^{5/3})/\partial x_e$ vary substantially in a limited region. We find that, if $\partial(pV^{5/3})/\partial x_e$ varies in that region but remains negative everywhere, then the buoyancy frequency can vary substantially but remains real (indicating a stable configuration). If $\partial(pV^{5/3})/\partial x_e$ is positive in a small region, then the buoyancy frequency can be imaginary, indicating a local instability. If $\partial(pV^{5/3})/\partial x_e$ is small but negative, then the buoyancy frequency agrees with interchange calculations, even in the inner magnetosphere. Except for some notable locations inside the bubble, the three approaches agree in their prediction of the buoyancy frequencies.

A main result suggested by our findings is that in the presence of bubbles, which frequently show up in the region during any substorm expansion phase, the agreement between the MHD and the pure interchange treatment is restored where previous average magnetosphere results showed a disparity. Our interpretation of these results is that the pure interchange treatment is more reasonable in the inner plasma sheet and inner magnetosphere when the magnetotail is disturbed, as compared to an average quiet-time magnetosphere.

Acknowledgments

This work is supported by NASA TMS grant 80NSSC20K1276.

Open Research

Model code and simulation results used in this paper are available at: 10.5281/zenodo.10909015.

References

Angelopoulos, V., Baumjohann, W., Kennel, C. F., Coroniti, F. V., Kivelson, M. G., Pellat, R., et al. (1992). Bursty bulk flows in the inner central plasma sheet. *Journal of Geophysical Research: Space Physics*, 97(A4), 4027–4039. https://doi.org/10.1029/91JA02701

Angelopoulos, V., Kennel, C. F., Coroniti, F. V., Pellat, R., Kivelson, M. G., Walker, R. J., et al. (1994). Statistical characteristics of bursty bulk flow events. *Journal of Geophysical Research: Space Physics*, *99*(A11), 21257–21280. https://doi.org/10.1029/94JA01263

Apatenkov, S. V., Sergeev, V. A., Kubyshkina, M. V., Nakamura, R., Baumjohann, W., Runov, A., Alexeev, I., Fazakerley, A., Frey, H., Muhlbachler, S., Daly, P. W., Sauvaud, J.-A., Ganushkina, N., Pulkkinen, T., Reeves, G. D., and Khotyaintsev, Y.(2007). Multi-spacecraft observation of plasma dipolarization/injection in the inner magnetosphere, *Annales de Geophysique,* 25, 801–814, https://doi.org/10.5194/angeo-25-801-2007

Bernstein, I. B., Frieman, E. A., Kruskal, M. D., & Kulsrud, R. (1958). An energy principle for hydromagnetic stability problems. *Proceedings of the Royal Society of London. Series A. Mathematical and Physical Sciences*, *244*(1236), 17–40. https://doi.org/10.1098/rspa.1958.0023

Birn, J., Raeder, J., Wang, Y. L., Wolf, R. A., & Hesse, M. (2004). On the propagation of bubbles in the geomagnetic tail. *Annales de Geophysique,* 22, 1773–1786. https://doi.org/10.1002/jgra.50521

Chen, C. X., & Wolf, R. A. (1993). Interpretation of high-speed flows in the plasma sheet. *Journal of Geophysical Research: Space Physics*, *98*(A12), 21409–21419. https://doi.org/10.1029/93JA02080

Chen, C. X., & Wolf, R. A. (1999). Theory of thin-filament motion in Earth's magnetotail and its application to bursty bulk flows. Journal of Geophysical Research: Space Physics, 104(A7), 14613–14626. https://doi.org/10.1029/1999JA900005

Cramer, W. D., Raeder, J., Toffoletto, F. R., Gilson, M., & Hu, B. (2017). Plasma sheet injections into the inner magnetosphere: Two-way coupled OpenGGCM-RCM model results. *Journal of Geophysical Research: Space Physics*, *122*(5), 5077–5091. https://doi.org/10.1002/2017JA024104

Dubyagin, S., Sergeev, V., Apatenkov, S., Angelopoulos, V., Runov, A., Nakamura, R., et al. (2011). Can flow bursts penetrate into the inner magnetosphere? *Geophysical Research Letters*, *38*(8). https://doi.org/10.1029/2011GL047016

Gallagher, D. L., Craven, P. D., & Comfort, R. H. (2000). Global core plasma model. *Journal of Geophysical Research: Space Physics*, *105*(A8), 18819–18833. https://doi.org/10.1029/1999JA000241

607 Erickson, G. M., & Wolf, R. A. (1980). Is steady convection possible in the Earth's
608 magnetotail? *Geophysical Research Letters*, 7(11), 897–900.
609 https://doi.org/10.1029/GL007i011p00897

610 Hsu, T.-S., & McPherron, R. L. (2007). A statistical study of the relation of Pi2 and plasma
611 flows in the tail. *Journal of Geophysical Research,* 112,
612 A05209. https://doi.org/10.1029/2006JA011782

613 Hu, B., Wolf, R. A., Toffoletto, F. R., Yang, J., & Raeder, J. (2011). Consequences of
614 violation of frozen-in-flux: Evidence from OpenGGCM simulations. *Journal of*
615 *Geophysical Research: Space Physics*, *116*(A6).
616 https://doi.org/10.1029/2011JA016667

617 Hurricane, O. (1994). The Kinetic Theory and Stability of a Stochastic Plasma with Respect
618 to Low Frequency Perturbations and Magnetospheric Convection, PhD Thesis,
619 UCLA.

620 Hurricane, O. A., Pellat, R., & Coroniti, F. V. (1994). The kinetic response of a stochastic
621 plasma to low frequency perturbations. *Geophysical Research Letters*, *21*(4), 253–
622 256. https://doi.org/10.1029/93GL03533

623 Lemon, C., Toffoletto, F., Hesse, M., & Birn, J. (2003). Computing magnetospheric force
624 equilibria. *Journal of Geophysical Research: Space Physics*, *108*(A6).
625 https://doi.org/10.1029/2002JA009702

626 Lui, A. T. Y., McEntire, R. W., & Krimigis, S. M. (1987). Evolution of the ring current
627 during two geomagnetic storms. *Geophysical Research Letters*, *92*(A7), 7459–7470.
628 https://doi.org/10.1029/JA092iA07p07459

629 Panov, E. V., Kubyshkina, M. V., Nakamura, R., Baumjohann, W., Angelopoulos, V.,
630 Sergeev, V. A., & Petrukovich, A. A. (2013). Oscillatory flow braking in the
631 magnetotail: THEMIS statistics. *Geophysical Research Letters*, *40*(11), 2505–2510.
632 https://doi.org/10.1002/grl.50407

633 Pembroke, A., Toffoletto, F., Sazykin, S., Wiltberger, M., Lyon, J., Merkin, V., & Schmitt,
634 P. (2012). Initial results from a dynamic coupled magnetosphere-ionosphere-ring
635 current model. *Journal of Geophysical Research: Space Physics*, *117*(A2).
636 https://doi.org/10.1029/2011JA016979

637 Petrashchuk, A., Mager, P., & Klimushkin, D. (2022). Numerical analysis of the spatial
638 structure of Alfvén waves in a finite pressure plasma in a dipole magnetosphere.
639 *Solar-Terrestrial Physics*, *8*(3), 3–12. https://doi.org/10.12737/stp-83202201

640 Pontius, D. H., & Wolf, R. A. (1990). Transient flux tubes in the terrestrial magnetosphere.
641 *Geophysical Research Letters*, *17*(1), 49–52.
642 https://doi.org/10.1029/GL017i001p00049

643 Sergeev, V. A., Angelopoulos, V., Gosling, J. T., Cattell, C. A., and Russell, C.
644 T. (1996), Detection of localized, plasma-depleted flux tubes or bubbles in the
645 midtail plasma sheet, Journal of Geophysical Research, 101(A5), 10817–10826,
646 https://doi.org/10.1029/96JA00460

647 Sergeev, V. A., Chernyaev, I. A., Angelopoulos, V., Runov, A. V., & Nakamura, R. (2014).
648 Stopping flow bursts and their role in the generation of the substorm current wedge.
649 *Geophysical Research Letters*, *41*(4), 1106–1112.
650 https://doi.org/10.1002/2014GL059309

651 Sorathia, K. A., Michael, A., Merkin, V. G., Ukhorskiy, A. Y., Turner, D. L., Lyon, J. G., et
652 al. (2021). The Role of Mesoscale Plasma Sheet Dynamics in Ring Current
653 Formation. *Frontiers in Astronomy and Space Sciences*, *8*, 192.
654 https://doi.org/10.3389/fspas.2021.761875

655 Spence, H. E., Kivelson, M. G., Walker, R. J., & McComas, D. J. (1989). Magnetospheric
656 plasma pressures in the midnight meridian: Observations from 2.5 to 35 R_E. *Journal*
657 *of Geophysical Research*, *94*(A5), 5264. https://doi.org/10.1029/JA094iA05p05264

658 Toffoletto, F. R., Wolf, R. A., & Schutza, A. M. (2020). Buoyancy Waves in Earth's
659 Nightside Magnetosphere: Normal-Mode Oscillations of Thin Filaments. *Journal of*
660 *Geophysical Research: Space Physics*, *125*(1).
661 https://doi.org/10.1029/2019JA027516

662 Toffoletto, F. R., Wolf, R. A., & Derr, J. (2022). Thin Filaments in an Average
663 Magnetosphere: Pure Interchange Versus Ballooning Oscillations. *Journal of*
664 *Geophysical Research: Space Physics*, *127*(10).
665 https://doi.org/10.1029/2022JA030556

666 Tsyganenko, N. A. (1987). Global quantitative models of the geomagnetic field in the
667 cislunar magnetosphere for different disturbance levels. *Planetary and Space*
668 *Science*, *35*(11), 1347–1358. https://doi.org/10.1016/0032-0633(87)90046-8

669 Tsyganenko, N. A., & Mukai, T. (2003). Tail plasma sheet models derived from Geotail
670 particle data. *Journal of Geophysical Research: Space Physics*, *108*(A3).
671 https://doi.org/10.1029/2002JA009707

672 Wang, C., Xing, X., Bortnik, J., & Chu, X. (2020). Inward Propagation of Flow-Generated
673 Pi2 Waves from the Plasma Sheet to the Inner Magnetosphere. *Journal of*
674 *Geophysical Research: Space Physics*, *125*(2), e2019JA027581.
675 https://doi.org/10.1029/2019JA027581

676 Wiltberger, M., Merkin, V., Lyon, J. G., & Ohtani, S. (2015). High-resolution global
677 magnetohydrodynamic simulation of bursty bulk flows. *Journal of Geophysical*
678 *Research: Space Physics*, *120*(6), 4555–4566.
679 https://doi.org/10.1002/2015JA021080

680 Wolf, R. A., Kumar, V., Toffoletto, F. R., Erickson, G. M., Savoie, A. M., Chen, C. X., &
681 Lemon, C. L. (2006). Estimating local plasma sheet $PV^{5/3}$ from single-spacecraft
682 measurements. *Journal of Geophysical Research: Space Physics*, *111*(A12),
683 2006JA012010. https://doi.org/10.1029/2006JA012010

684 Wolf, R. A., Wan, Y., Xing, X., Zhang, J.-C., & Sazykin, S. (2009). Entropy and plasma
685 sheet transport. *Journal of Geophysical Research: Space Physics*, *114*(A9),
686 https://doi.org/10.1029/2009JA014044

687 Wolf, R. A., Chen, C. X., & Toffoletto, F. R. (2012). Thin filament simulations for Earth's
688 plasma sheet: Interchange oscillations. *Journal of Geophysical Research: Space*
689 *Physics*, *117*(A2). https://doi.org/10.1029/2011JA016971

690 Xing, X., & Wolf, R. A. (2007). Criterion for interchange instability in a plasma connected
691 to a conducting ionosphere. *Journal of Geophysical Research: Space Physics* 112,
692 A12209. https://doi.org/10.1029/2007JA012535

693 Xing, X., Wang, C.-P., Liang, J., & Lyons, L. R.(2015). Plasma sheet Pi2 pulsations
694 associated with bursty bulk flows, *Journal of Geophysical Research: Space*
695 *Physics*, 120, 8692–8706. https://doi.org/10.1002/2015JA021668

696 Yang, J., Toffoletto, F. R., Erickson, G. M., & Wolf, R. A. (2010). Superposed epoch study
697 of $PV^{5/3}$ during substorms, pseudobreakups and convection bays. *Geophysical*
698 *Research Letters*, *37*, L07102. https://doi.org/10.1029/2010GL042811

699 Yang, J., Wolf, R. A., Toffoletto, F. R., Sazykin, S., & Wang, C.-P. (2014). RCM-E
700 simulation of bimodal transport in the plasma sheet. *Geophysical Research Letters*,
701 *41*(6), 1817–1822. https://doi.org/10.1002/2014GL059400

702 Xia, Z., Chen, L., Zheng, L., & Chan, A. A. (2017). Eigenmode analysis of compressional
703 poloidal modes in a self-consistent magnetic field. *Geophysical Research Letters*,
704 *122*(10), 10,369-10,381. https://doi.org/10.1002/2017JA024376